NeuroImage: Clinical 30 (2021) 102579

Contents lists available at ScienceDirect

NeuroImage: Clinical

journal homepage: www.elsevier.com/locate/ynicl

MR Elastography demonstrates reduced white matter shear stiffness in early-onset hydrocephalus

M.E. Wagshul [a,*], J.P. McAllister [b], D.D. Limbrick Jr. [b,c], S. Yang [a], W. Mowrey [d], J.T. Goodrich [e], A. Meiri [a], D.M. Morales [b], A. Kobets [e], R. Abbott [e]

[a] Albert Einstein College of Medicine, Gruss MRRC, Departments of Radiology and Physiology & Biophysics, Bronx, NY, USA
[b] Saint Louis Children's Hospital and the Department of Neurosurgery, Washington University School of Medicine, Saint Louis, MO, USA
[c] Department of Pediatrics, Washington University, School of Medicine, USA
[d] Albert Einstein College of Medicine, Department of Epidemiology and Population Health, Bronx, NY, USA
[e] Montefiore Medical Center, Department of Neurosurgery, Bronx, NY, USA

ARTICLE INFO

Keywords:
Pediatric hydrocephalus
Shunting
MR Elastography
White matter stiffness
Shear stiffness
Quality of life

ABSTRACT

Introduction: Hydrocephalus that develops early in life is often accompanied by developmental delays, headaches and other neurological deficits, which may be associated with changes in brain shear stiffness. However, noninvasive approaches to measuring stiffness are limited. Magnetic Resonance Elastography (MRE) of the brain is a relatively new noninvasive imaging method that provides quantitative measures of brain tissue stiffness. Herein, we aimed to use MRE to assess brain stiffness in hydrocephalus patients compared to healthy controls, and to assess its associations with ventricular size, as well as demographic, shunt-related and clinical outcome measures.

Methods: MRE was collected at two imaging sites in 39 hydrocephalus patients and 33 healthy controls, along with demographic, shunt-related, and clinical outcome measures including headache and quality of life indices. Brain stiffness was quantified for whole brain, global white matter (WM), and lobar WM stiffness. Group differences in brain stiffness between patients and controls were compared using two-sample t-tests and multivariable linear regression to adjust for age, sex, and ventricular volume. Among patients, multivariable linear or logistic regression was used to assess which factors (age, sex, ventricular volume, age at first shunt, number of shunt revisions) were associated with brain stiffness and whether brain stiffness predicts clinical outcomes (quality of life, headache and depression).

Results: Brain stiffness was significantly reduced in patients compared to controls, both unadjusted ($p \leq 0.002$) and adjusted ($p \leq 0.03$) for covariates. Among hydrocephalic patients, lower stiffness was associated with older age in temporal and parietal WM and whole brain (WB) (beta (SE): −7.6 (2.5), $p = 0.004$; −9.5 (2.2), $p = 0.0002$; −3.7 (1.8), $p = 0.046$), being female in global and frontal WM and WB (beta (SE): −75.6 (25.5), $p = 0.01$; −66.0 (32.4), $p = 0.05$; −73.2 (25.3), $p = 0.01$), larger ventricular volume in global, and occipital WM (beta (SE): −11.5 (3.4), $p = 0.002$; −18.9 (5.4), $p = 0.0014$). Lower brain stiffness also predicted worse quality of life and a higher likelihood of depression, controlling for all other factors.

Conclusions: Brain stiffness is reduced in hydrocephalus patients compared to healthy controls, and is associated with clinically-relevant functional outcome measures. MRE may emerge as a clinically-relevant biomarker to assess the neuropathological effects of hydrocephalus and shunting, and may be useful in evaluating the effects of therapeutic alternatives, or as a supplement, of shunting.

Abbreviations: ANTs, Anatomical Normalization Tools; BDI, Beck's Depression Inventory; CDI, Child's Depression Inventory; CSF, cerebrospinal fluid; DTI, diffusion tensor imaging; ETV, endoscopic third ventriculostomy; HOQ, hydrocephalus outcome questionnaire; IQR, Interquartile range; ICP, intracranial pressure; ICV, intracranial volume; IVH, Intraventricular hemorrhage; MRE, Magnetic Resonance Elastography; MDEV, multi-frequency dual elasto-visco; OSS, octahedral shear strain; QoL, quality of life; SLCH, Saint Louis Children's Hospital; VVR, ventricular volume ratio; WM, white matter; WB, whole brain.

* Corresponding author.
E-mail address: mark.wagshul@einsteinmed.org (M.E. Wagshul).

https://doi.org/10.1016/j.nicl.2021.102579
Received 7 August 2020; Received in revised form 8 December 2020; Accepted 21 January 2021
Available online 2 February 2021

1. Introduction

Hydrocephalus is a condition characterized by abnormal dilatation of the cerebral ventricles, typically as a result of an imbalance between the rates of production and absorption of cerebrospinal fluid (CSF) (Leinonen et al., 2017; Bergsneider et al., 2006). This imbalance can be the product of either an overt blockage to CSF outflow from the ventricles, *i.e.,* non-communicating hydrocephalus, or a downstream blockage elsewhere in the flow pathway, *i.e.,* communicating hydrocephalus where the lateral ventricles communicate with the subarachnoid spaces. Hydrocephalus often occurs early in life and if left untreated can result in elevated intracranial pressure (ICP), structural distortion of the brain (Yuan et al., 2016; Rajagopal et al., 2013; Tan et al., 2018; Hofmann et al., 1995), compression or stretching of the periventricular white matter (WM) (Jang et al., 2013; Yuan et al., 2013), cortical thinning (Kang et al., 2018; Zhang et al., 2017), and impaired blood flow and abnormal capillary vessel density and caliber (Luciano et al., 2001), all of which can contribute to severe brain damage or death. CSF diversion is the mainstay of treatment, but does not address the root cause of the ventricular dilatation, and either requires implantation of a permanent diversion device (*e.g.*, ventriculo-peritoneal shunt) which will remain for the lifetime of the patient or internal CSF diversion (*e.g.,* endoscopic third ventriculostomy, ETV). Unfortunately, there are likely long-term effects of CSF diversion, in addition to the primary insult from the initial ventricular dilatation and subsequent insults at the time of shunt malfunction or failure. The long-term effects of hydrocephalus and shunting include deficits in cognitive (Lacy et al., 2008), motor (Houtrow et al., 2018), and behavioral skills (Boyer et al., 2006), as well as their downstream effect on school performance, employability and quality of life (Gmeiner et al., 2019; Gigi et al., 2019; Kao et al., 2001; Fletcher et al., 2002).

For the last twenty years, investigators have attempted to identify noninvasive biomarkers for gauging changes in the hydrocephalic brain as well as for guiding development of potential alternative therapies. Radiologically, the size of the lateral ventricles may not be directly or solely related to prognosis; it is well known, for example, that the ventricles will not always decrease in size following shunt surgery or ETV, even in the presence of marked clinical improvement, and may not always dilate with shunt failure (Buxton et al., 1998; Nikas et al., 2014; Patra et al., 2016; Kim et al., 2000). CSF flow imaging, and in particular pulsatility through the cerebral aqueduct, has received much attention although mostly in adult hydrocephalus, and even there, conclusions are mixed (Luetmer et al., 2002; Bradley et al., 1996; Mouton Paradot et al., 2010; Kahlon et al., 2007). Diffusion tensor imaging (DTI) has shown promise for demonstrating WM changes, and has been used to show loss of WM integrity in both periventricular (Yuan et al., 2013, 2009; Assaf et al., 2006) as well as more distal structures (Tan et al., 2018; Ben-Sira et al., 2015). Most of these results however were in acute hydrocephalus. In this work, we sought to identify an imaging-based biomarker of brain pathology in patients with long-standing, stable, shunted hydrocephalus.

MR Elastography (MRE) is a relatively new, noninvasive technique for measuring brain tissue stiffness, and has demonstrated softening of brain tissue in a wide variety of neurological diseases (Wuerfel et al., 2010; Yin et al., 2018; Murphy et al., 2013). MRE has distinct advantages over prior methods for assessing intracranial compliance or stiffness – as a noninvasive method it will be more easily accessible to all patients, and as an imaging method, it provides detailed, localized metrics of brain stiffness which can be compared to healthy brains, across patient groups or longitudinally in individual patients. This technique is particularly attractive for studying brain changes in hydrocephalus because of the numerous biomechanical effects present: 1) the hydrocephalus itself causes structural distortion of nearby structures and in more severe cases cortical compression, 2) even following successful CSF diversion (*i.e.*, stable prognosis), the ventricles can be moderately enlarged or dysmorphic, 3) there is evidence of ultrastructural changes at the capillary level – changes in perfusion have been shown to lead to alterations in brain stiffness (Hetzer et al., 2018), presumably through changes in perfusion pressure or biomechanical changes in the vasculature, 4) there is evidence of changes in brain compliance (where compliance = 1/elastance, typically measured with an infusion test, which assesses global stiffness of the intracranial system), and 5) there are changes in fluid balance and pressure regulation likely accompanied by both local and global changes in brain tissue stiffness. In this work, we sought to validate MRE as a viable noninvasive method for assessing differences in brain stiffness in children and adults with long-standing, stable, shunted, early-onset hydrocephalus compared to healthy controls, and to assess among patients which factors are associated with brain stiffness, and whether brain stiffness predicts clinically-relevant outcomes including quality of life, headache and depression. Our hypothesis was that hydrocephalus patients would demonstrate decreased brain stiffness compared to healthy controls, and that reduced brain stiffness in patients would be correlated with impaired clinical outcome.

2. Methods

2.1. Subjects

Hydrocephalus patients were identified through chart review, at the time of routine clinical visits with the study neurosurgeons (R.A., J.G. and D.L.), and through social media (Facebook, and website of the Hydrocephalus Association) at two study sites, Albert Einstein College of Medicine in New York, and Washington University School of Medicine/Saint Louis Children's Hospital (SLCH). Most of the patients identified through chart review had a recorded history of headache, although current or past headache history was not an inclusion or exclusion criterion for the study. All patients had a non-programmable shunt, with their first shunt implanted at < 2 years of age and were clinically stable; the most recent clinically-relevant event (*e.g.,* shunt revision) was 9 months prior to recruitment (mean = 9.4 yrs). Healthy controls were recruited by advertisement in the local area and had no history of neurological disease or head trauma.

The HIPPA compliant study protocol was approved by each local Internal Review Board and informed consent/assent was obtained from all subjects or their parent/guardian prior to enrollment.

2.2. Demographics and clinical data

Hydrocephalus patients completed a REDCap electronic data capture questionnaire (Harris et al., 2009) consisting of questions related to medical history, quality of life and headache symptoms. Healthy controls did not provide any survey data but were screened for absence of prior neurological disease and history of headache. Clinical data included hydrocephalus etiology, age at first shunt, revision history, and medication usage. Functional clinical outcome was assessed with headache, quality of life and depression measures. Headache scores used the Headache Disability Inventory (HDI), a 25 question instrument covering both social/emotional and physical effects of headache on quality of life (Jacobson et al., 1995). HDI scores range from 0 to 100 where higher score represents higher headache severity or impact on daily life. Overall quality of life was assessed with the Hydrocephalus Outcome Questionnaire (HOQ) which provides health-related quality of life (QoL) information, from 4 weeks prior to the visit, in physical, emotional and cognitive domains and has been shown to have excellent test–retest reliability, interrater reliability and internal consistency (Kulkarni et al., 2004, 2008; Platenkamp et al., 2007). HOQ scores range from 0 to 1 with higher scores indicating better quality of life. Depression was assessed with Beck's Depression Inventory (BDI) for adults (Wang and Gorenstein, 2013) and Child's Depression Inventory (CDI) for children (Kovacs, 1985; Thabrew et al., 2017). A depression cut score of 20 was used for presence or absence of depression (Wang and

Gorenstein, 2013; Bang et al., 2015). Headache, quality of life and depression data were only available for the Einstein cohort.

2.3. MRE vibration apparatus

MR Elastography relies on application of an external, microscopic vibration of the tissue of interest, the brain in our case, and a motion-sensitive MRI sequence synchronized with these vibrations (Kruse et al., 2008; Manduca et al., 2001). While the imaging voxels used in MRE are on the order of a few millimeters, the motion sensitivity produced within these voxels is on the order of microns, which allows quantification of discrete brain tissue regions with good tolerability to the procedure in children. The motion sensitivity is mapped onto the phase of the MRI signal, and a typical MRE sequence has a sensitivity of 0.5 rad per micron. Given a phase noise level of 0.1 rad or less, brain motion down to a few tenths of a micron can be detected. Thus, it is important to note that the vibrations which are generated and detected for an MRE scan are microscopic and well below the safety standards for vibration set by the US Occupational Safety and Health Administration (Ehman et al., 2008). The passive part of our MRI-compatible, MRE actuation system is shown in Fig. 1, and relies on two spring-loaded, pneumatically-driven polycarbonate pistons (U.S. Pat. 10694973). The pistons mount directly onto the rungs of an 8-channel MRI head coil and are fixed in place with a series of screws once the piston has been spring loaded against the zygomatic arch (*i.e.,* the cheekbone). Rubber pads on the end of the piston ensure a comfortable fitting for the patient. Each piston is driven by separate acoustic subwoofers (Definitive Technologies Prosub 1000, with a 10″ woofer, 300-watt amplifier and 18–150 Hz frequency response), driven by a digital function generator (Stanford Research Systems, DS345), located outside the MRI room and coupled via a ~ 20 foot long plastic tube. The speakers are driven out-of-phase to produce a gentle right-to-left rocking motion of the head.

With respect to optimal delivery of vibrations to the head, adequate loading of the piston springs was important to ensure high quality data as well as patient comfort. With suboptimal loading, the pistons successively engage and disengage from the cheekbone with each vibration, producing a more jarring motion. This is uncomfortable for the patient and produces higher harmonics in the brain waves which are not useful in the reconstruction (the first step in our reconstruction is to throw out everything but the fundamental vibration at 30 Hz), and can corrupt the elastance maps because these harmonics have a different spatial pattern than the fundamental wave (through aliasing, (Clayton et al., 2013; Fovargue et al., 2018; Venkatesh et al., 2013). Once the springs are loaded, however, the pistons create a smooth motion, transmitting almost exclusively the fundamental vibration frequency, with a very comfortable experience for the patient.

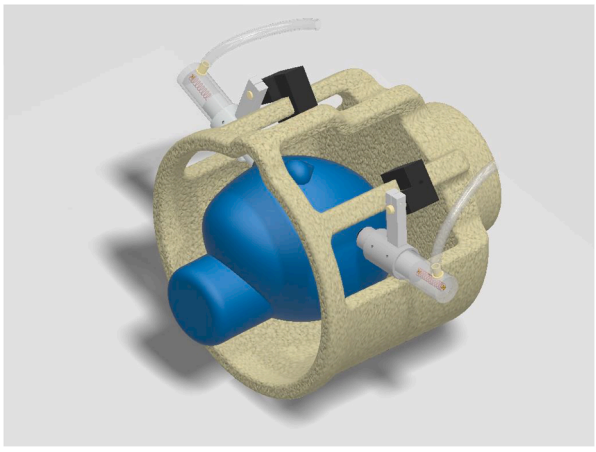

Fig. 1. Depiction of the MRE vibration actuator inside the MRI head coil. The two spring-loaded, pneumatically-driven, MRI-compatible pistons are driven out of the phase at 30 Hz to produce a gentle, side-to-side rocking of the head. Net skull motion is < 1 mm.

In a small subset of subjects (2 patients and 2 controls), the actuator device was replaced with soft pillows situated on the sides of the head. This was due to a change in the MRI head coil which could not accommodate the pistons. However, in all of these subjects, wave patterns and octahedral shear strain signal-to-noise ratio (OSS-SNR, see below, section 2.4) values similar to those in other subjects were obtained.

2.4. MRI acquisition

Imaging at Einstein was performed on a 3T Philips scanner (Achieva TX, Philips Medical Systems, Best, The Netherlands), and at SLCH on a 3T Siemens Prisma (Siemens Medical Systems, Erlangen, Germany), with an 8-channel head coil. MRE data were acquired in 30 axial slices oriented along the AC-PC line, using a phase-sensitive, single-shot, spin echo EPI sequence with the following parameters (where two values are given, they refer to the Einstein/SLCH sites respectively): TE: 67–96/100 ms, TR: 4/8–10 s, voxel size: 2.5/2.5–3 mm isotropic, vibration frequency: 30/30–31.25 Hz, and 8 MRE frames collected over the vibration cycle. Motion-encoding gradients were applied with the following parameters: amplitude: 53/70 mT/m, 32–33.3 ms in length and with a trapezoidal shape; encoding gradients were applied on each side of the 180° pulse, separated by 1 vibration cycle (32–33.3 ms). Six MRE images were collected with vibration sensitization along ± x, ±y, and ± z, with these directions being relative to the imaging plane (*i.e.,* x = right-left, y = anterior-posterior, z = foot-head). Total acquisition time was approximately 4 min. Magnitude images were used for motion and EPI-distortion corrections, as well as registration of MRE images to the T1 anatomical reference, while phase images were used to extract the vibration-induced wave motion. It should be noted that there were some significant differences in the image acquisition parameters for the two scanners, as well as those due to changes in scanner software over the data collection period. However, because of the need for external vibration of the brain and wide subject-to-subject variability in transmission of these vibrations to the brain (*e.g.,* coupling of the actuator to the head, head size and mass), these differences were not expected to affect the data analysis. Nonetheless, each set of MRE wave images needs to be of adequate quality to ensure good reconstruction of elastance maps. Thus, for each scan, wave images were reviewed both visually and quantitatively to ensure adequate quality for reconstruction. Quantitative assessments used the OSS-SNR (McGarry et al., 2011) averaged over the entire brain, with a threshold of OSS-SNR > 3.0 for acceptance of the data as has been used in prior MRE work (see *e.g.,* (Arunachalam et al., 2017; Johnson et al., 2013).

High resolution T1-weighted images (MPRAGE, TE/TR/TI = 4.6/9.9/900 ms, and voxel size − 1 mm isotropic) were acquired to provide segmentation of anatomical regions of interest. Field map images (gradient echo, TE/TE/TR = 2.4/2.3/20 ms, voxel size 4 mm isotropic) were collected to correct for EPI-related distortion, as well as FLAIR images to quantify WM hyperintensities.

2.5. Image processing

Because MRE reconstruction relies on inversion of the equations of motion based on MRI-derived images of microscopic tissue movement, fidelity in the spatial relationships within the MRE images is critical. This is at odds with the spatial distortion inherent in the single-shot EPI image acquisition needed to collect all of the MRE data within a reasonable time period. We therefore took great care to ensure optimal post-processing of the MRE images prior to submission to inversion. Correction steps were carried out on the real and imaginary parts of the MRE signal because the phase of the MRE signal (which contain the tissue motion information) can be corrupted by post-processing steps

(Fehlner et al., 2017). Our processing stream included: 1) brain extraction (Lutkenhoff et al., 2014), 2) initial phase unwrapping, 3) conversion to real/imaginary images, 4) motion correction, 5) correction of EPI-related field distortions, 6) conversion back to phase images, 7) combination of the positive and negative phase images (*e.g.,* +x and -x) and 8) final unwrapping of phase aliasing. Motion corrections of the magnitude images were performed with MCFLIRT, part of the FSL library (Smith et al., 2004) and then applied to the real and imaginary datasets. EPI-distortion corrections were calculated using FSL's epi_reg routine, and the output warp fields were then applied to the MRE images (magnitude, real and imaginary) to correct field-induced distortions. Phase image unwrapping used 2D Gaussian denoising of the complex MRI data with 5-pixel edge size and $\sigma = 0.65$ followed by derivative-based unwrapping (Hirsch et al., 2017).

Ventricular size was quantified as ventricular volume divided by total intracranial volume (ICV). Ventricular volume (VV) was isolated as the ventricular portion of the CSF component from FAST segmentation (part of FSL's FMRIB's Automated Segmentation Tool, (Zhang et al., 2001). Intracranial volume was calculated as the total of all three components (GM + WM + CSF). Ventricular volume measures thus are cited as the ventricular volume ratio, VVR = VV/ICV.

The entire MRE reconstruction pipeline is publicly available at https://bioqic-apps.charite.de, and follows the methodology adopted in (Streitberger et al., 2014): a) two images of in-plane strain components are obtained for each vibration sensitization direction, b) temporal Fourier transformation to generate six complex-valued wave derivative images, c) a second noise suppression using a 2D Butterworth lowpass filter with a threshold of 100 m^{-1}. Wave denoising was applied before each spatial derivative operation to minimize derivative-related noise augmentation (Hirsch et al., 2017). Finally, the wave images were inverted by multi-frequency dual elasto-visco (MDEV) inversion, as applied to single frequency data (Hirsch et al., 2014). MDEV inversion provides high-resolution maps of the complex-valued shear modulus, G*. The magnitude of the shear modulus, |G*|, is a lumped parameter of viscoelasticity which quantifies both storage and loss properties (Guo et al., 2013; Braun et al., 2014). One should note that changes in |G*| can be related to both elasticity and viscosity. The general term "stiffness" or "shear stiffness" is often used in the literature to refer to |G*|; this convention has been adopted here. The units for stiffness are Pascal.

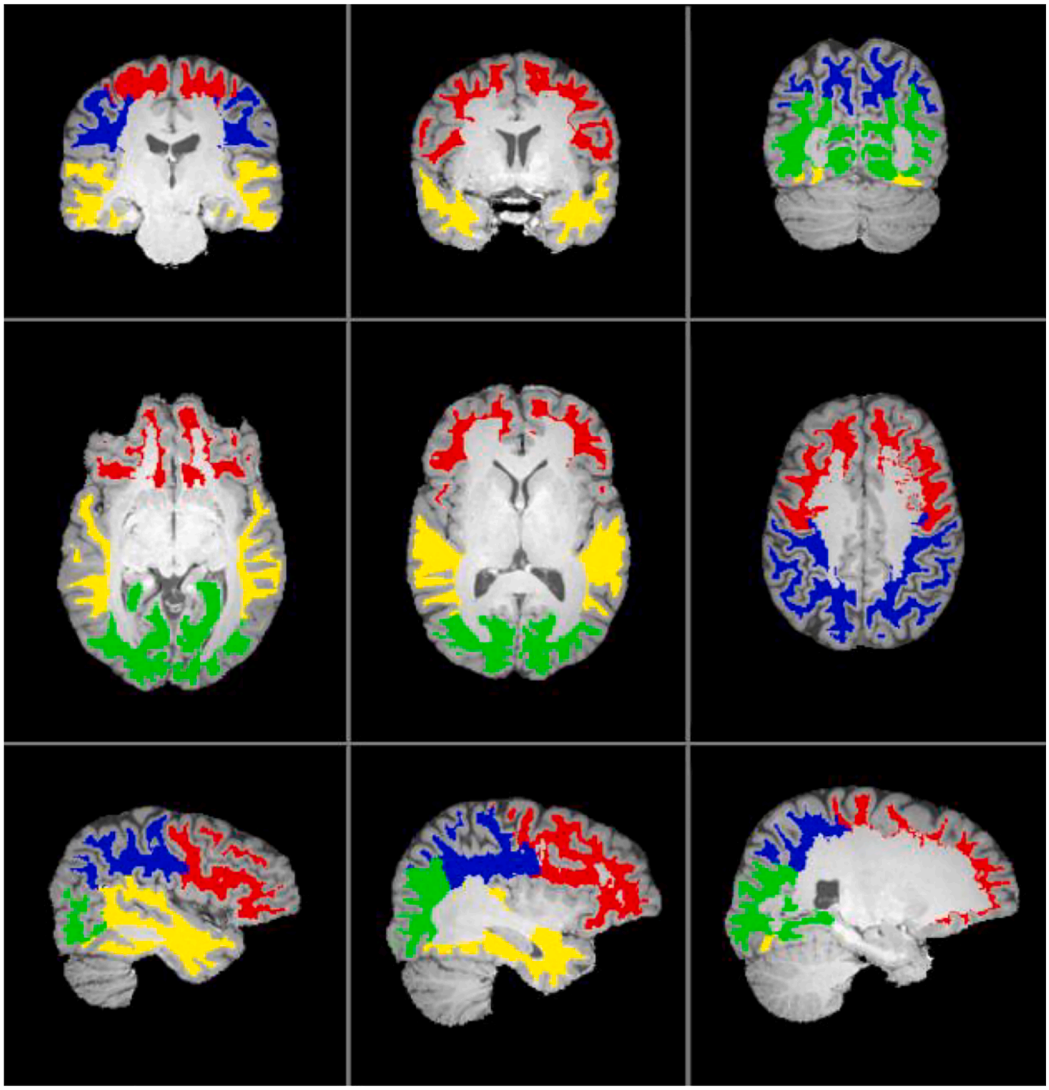

Fig. 2. Label regions corresponding to frontal (red), parietal (blue), occipital (green) and temporal (yellow) white matter from the MRICloud atlas which were used for extracting lobar white matter stiffness measures. Labels are overlaid on top of the T1 image of a control subject, and shown at three different levels in the coronal, axial and sagittal planes. (For interpretation of the references to color in this figure legend, the reader is referred to the web version of this article.)

2.6. Extraction of regional stiffness measures

Regional segmentation of the brain used the freely available MRICloud (https://mricloud.org/) (Oishi et al., 2009), which is a multi-atlas approach to brain segmentation performed on the T1 structural image, and results in a set of 283 unique labels. Although many of our subjects were younger, we obtained good segmentation results with the 26 atlas, age 22–50 pipeline (*e.g.* visual inspection of segmentation indicated good overlap between T1 and atlas structures), so this was maintained for all subjects. Labels identify cortical and subcortical grey matter, a subset of WM structures (*e.g.,* corpus callosum, internal capsule and corona radiata), and a detailed table is available for grouping of structures based on anatomical location (*e.g.,* frontal vs. parietal structures). Because of the non-local nature of MRE stiffness estimate, *i.e.,* stiffness measures can be affected by nearby pixels, dilated CSF maps (3 pixel kernel) were used for all calculations as a mask to exclude pixels with CSF contamination. Labeling was done in subject space, rather than atlas space to account for distortions in anatomy and so that label maps could be directly morphed onto the MRE images using the output transformation matrices to yield regional measures of stiffness; regions were limited to WM and identified by lobar label, *i.e.,* frontal, parietal, occipital and temporal WM. Label regions are illustrated overlaid on the T1 image of a control subject in Fig. 2. Whole brain stiffness, including both white and grey matter, was also extracted.

2.7. Visualization of mean stiffness distributions

The results provided below allowed statistical comparisons between hydrocephalus patients and healthy controls for identifying potential differences in stiffness at various locations in the brain. However, we surmised that a visual representation of the biomechanical structure of the brain, and how that structure might change with a disease such as hydrocephalus, would be helpful for better appreciating the significance of our results. To this end, we used the following procedure to average control and patient MRE maps into a common anatomical space: 1) Registration of each individual MRE map to its T1 structural image, using FSL FLIRT, with 6 degrees of freedom, 2) registration of each individual T1 to a common study-specific template, using the ANTs package (Anatomical Normalization Tools, (Avants et al., 2011), and 3) application of the resultant transformation matrix to the T1-registered MRE image to produce a subject-specific MRE map in template space. The study-specific template was constructed using iterative ANTs registrations to produce an optimized template with minimum distortion and one which is most representative of the entire study population. Because of the obvious issues related to accurate warping of brain anatomy to the study template in the presence of severe ventricular distortion or dilatation or large shunt-related artifacts, patients with such anomalies were excluded from these analyses ($n = 6$). Once all appropriate patients and controls had been warped into template space, separate averages of patients and controls were calculated for qualitative comparison of brain stiffness features of the two populations.

2.8. Statistical analyses

Participant characteristics were compared between hydrocephalus patients and healthy controls using Wilcoxon rank sum test for continuous variables and Pearson's chi-squared test for categorical variables. The 2-sample *t*-test was used to assess whether brain stiffness was different in hydrocephalus patients compared to healthy controls. Multivariable linear regression models were used to assess whether brain tissue stiffness differs between patients and controls while adjusting for key potential confounders of age, sex, and VVR. Sensitivity analysis was conducted to further adjust for site as a covariate. Next, among the hydrocephalus patients alone, multivariable linear regression models were used to assess which factors (age, sex, VVR, age at first shunt, number of shunt revisions) were associated with brain tissue stiffness; age at first shunt and the number of shunt revisions were dichotomized according to those below/above the median. Finally, among the hydrocephalus patients with clinical functional outcome measures (quality of life, headache and depression, $n = 33$, Einstein site only), we assessed which demographic, brain volumetric or stiffness measures were associated with these clinical functional measures, using linear regression models for quality of life and headache index scores, and a logistic regression model for depression status. Statistical significance was set as $p < 0.05$, and all statistical analyses were performed in SAS 9.4 (SAS Institute Inc., Cary, NC, USA).

3. Results

Forty-seven (47) hydrocephalus patients and forty-four (44) controls were recruited into the study. Subjects were excluded from the final analysis as follows: Low OSS-SNR (<3, *i.e.,* poor MRE waves) 2/11 (patients/controls), subject could not tolerate MRI: 1 patient, excessive motion: 3 patients, equipment issues: 1 patient, and excessive shunt-related image artifacts: 1 patient. In only one case out of the 91 studies was the study halted because the subject was unable to tolerate the MRE vibrations. Thus, the final dataset consisted of 39 patients and 33 controls; across the two sites, there were 33 patients and 21 controls at the Einstein site and 6 patients and 12 controls at SLCH. Although there were differences between the two sites in age (Einstein: 21.5 ± 7.9, SLCH: 13.3 ± 4.0) and patient gender distribution (Einstein: 33% female, SLCH: 50% female), for each site individually there were no statistical differences between patients and controls in age or gender distribution. Collinearity between covariates revealed no significant associations.

Participant characteristics of the final analysis sample are summarized in Table 1. Age range was 9 to 39 years old for the patients and 6 to 46 years old for the controls with comparable medians ($p = 0.23$). Distribution of sex was comparable: 64.1% male vs. 45.5% female, $p = 0.11$. Total ventricular volume index median was numerically higher in patients but not significantly different from healthy controls ($p = 0.11$). Median ICV was significantly smaller in patients versus controls (median (IQR): 1752 (1639, 1923) vs. 1937 (1824, 2003), $p = 0.01$). Ventricular volume index when normalized by ICV, *i.e.,* the VVR, was larger in patients compared to controls ($p = 0.02$). Among patients alone, median age at first shunt was 120 days and median number of shunt revisions was 2.

Table 1 also shows the functional outcome measures for the Einstein patient group (HOQ, HDI, BDI/CDI). The headache index is primarily related to the effects of headache on daily activities, with the median score of 32.0 indicating moderate impact, although the scores spanned the full range (0–96). In contrast, median HOQ score (0.81) indicated good quality of life, with the major impact in cognitive and social-emotional domains. Scores ranged from fair to good, with no patients reporting severe impact on quality of life. There was a strong correlation between HOQ and HDI ($r = -0.55$), providing good internal validation of these clinical outcome measures. Finally, median depression score was 7, indicating mild to no depression for the patient group as a whole.

Fig. 3 shows representative wave images in a control and patient, demonstrating the typical wave quality in both subject groups. In Fig. 4, we depict the group-averaged shear stiffness maps; as noted above, while these were not used for any of the quantitative analysis below, they depict a coherent stiffness "structure" to the brain, in the same vein as WM tract depiction with DTI maps.

The overall group comparisons, without correction for covariates, demonstrated a significant decrease in brain stiffness both globally and regionally ($p \leq 0.002$) in the patient group. For whole brain WM, mean stiffness in patients was 959 ± 95 for patients vs. 1030 ± 55 for controls ($p = 0.0002$). Results can be found in Table 2. Univariable models, however, indicated significant associations between many of the demographic and volumetric measures and brain stiffness. For example, there was a significant correlation between lower brain stiffness and

Table 1
Participant characteristics.

	Hydrocephalus patients (n = 39)	Healthy controls (n = 33)	p-value
Age, years			
Mean (SD)	20.1 (7.0)	18.7 (8.9)	0.23
Median (IQR)	18 (16, 23)	16 (13, 24)	
Min — Max	9 — 39	6 — 46	
Female, n (%)	25 (64.1%)	15 (45.5%)	0.11
Total Ventricular volume (cc)			
Median (IQR)	14.7 (8.3, 33.8)	10.4 (7.4, 16)	0.11
Min — Max	2.8 — 269	3.9 — 39.3	
ICV (cc)			
Median (IQR)	1751.9 (1638.7, 1922.6)	1936.9 (1823.9, 2002.9)	0.01
Min — Max	1327.2 — 2674.6	1462.4 — 2332.9	
VVR (% of ICV)			
Median (IQR)	0.8 (0.5, 1.5)	0.5 (0.4, 0.8)	0.02
Min — Max	0.15 — 15.4	0.19 — 20	
Age at first shunt (mo)			
Median (IQR)	120 (14, 180)		
Min — Max	0 — 550		
Hydrocephalus cause (#)			
IVH	7		
Congenital	16		
Spina Bifida	4		
Other	4		
Unknown	8		
# shunt revisions, n (%)			
0	6 (15.4)		
1	11 (28.2)		
2	7 (18.0)		
3	3 (7.7)		
4 and up	12 (30.8)		
HOQ [b]			
Median (IQR)	0.81 (0.62, 0.84)		
Min — Max	0.43 — 0.94		
HDI [b]			
Median (IQR)	32 (22, 58)		
Min — Max	0 — 96		
Depression (n/%) [b]			
Moderate or severe	9 (27%)		
Minimal to none	24 (73%)		

IQR: Interquartile range; IVH: Intraventricular hemorrhage; HOQ: Hydrocephalus Outcome Questionnaire; HDI: Headache Disability Inventory (HDI); VVR: Ventricular volume ratio (VV/ICV).
[a]Wilcoxon rank sum test was used to compare continuous variables and Pearson's chi-squared test or Fisher's exact test was used to compare categorical variables between the groups.
[b] HOQ, HDI and Depression was only measured for the 33 patients at Einstein site.

increased ventricular size, such that patients with more severe ventricular dilation exhibited decreased brain stiffness (see Fig. 5A). There was also a significant association between WM stiffness and age (frontal, parietal and global WM, see Fig. 5B), wherein brain tissue softened with older age at a rate of ~ 50 Pa/decade, as well as with sex, wherein women exhibited softer brain tissue compared to men with a difference of ~ 50–70 Pa; see Fig. 5C.

The multivariable linear model was used to compare patients and controls while adjusting for age, sex and VVR for each of the six stiffness measures: whole brain, whole brain WM and 4 lobar WM ROIs (see Table 3): Brain stiffness remained significantly lower in patients compared to controls in all six stiffness measures (mean group difference range: 42.5–79.3; $p \leq 0.02$). Larger VVR was associated with lower stiffness in all regions except frontal lobe WM, older age was associated with lower stiffness in frontal, parietal and temporal WM and in whole brain stiffness, and women had lower stiffness compared to men in whole brain WM alone. All effects in Table 3 remained similar when further adjusting for site as a covariate.

Among patients alone, multivariable linear regression models were used to assess the associations between brain stiffness and age, sex, VVR, age at first shunt and number of shunt revisions, where age at first shunt was dichotomized at the median age (120 days) and number of shunt revisions was dichotomized at the median number (0–1 vs 2 +) (see Table 4). Older age remained associated with lower stiffness in parietal and temporal lobe WM, and whole brain stiffness. Compared to the results in Table 3, the sex estimate was more than double for this model including patients only, as well as the appearance of the significant sex effect in frontal lobe WM. Neither age at first shunt nor the number of shunt revisions were significant in explaining brain stiffness variance (p: 0.12—0.69). However, it should also be noted that the direction of the non-significant clinical parameters was always negative. All effects in Table 4 also remained similar when further adjusted for test site.

Finally, among the hydrocephalus patients with clinical functional outcome measures (n = 33, Einstein site only), we assessed the effects of age, sex, VVR, age at first shunt, number of shunt revisions, and stiffness measures on the functional outcome (Table 5). None of the demographic or clinical parameters, including ventricular size, were predictive of HOQ, HDI or depression; the one exception was the trend for a prediction of depression with age at first shunt, with younger age predicting lower likelihood of depression ($p = 0.06$). In contrast, higher stiffness in whole brain, global WM stiffness as well as in frontal (trend, $p = 0.07$) and parietal lobes were predictive of better health-related quality of life, but none of the WM stiffness measurements were associated with headache index. Higher whole brain, frontal and parietal WM, as well as WB stiffness were protective from depression (Odds ratio = 0.976, 95% CI: (0.953, 0.999), $p = 0.042$).

4. Discussion

The goals of this study were to: 1) demonstrate the feasibility of brain MRE for quantifying brain stiffness in children and adult hydrocephalus patients compared to controls, (2) investigate the differences in brain stiffness between hydrocephalus patients and healthy controls, and (3) assess potential associations in patients between brain stiffness and common clinical outcome parameters. Overall, we were able to obtain excellent quality vibration maps in a large percentage of patients and controls, with > 95% compliance with the procedure in subjects as young as 5 years old. Global WM measurements showed an overall ***decrease*** in brain stiffness in patients compared to controls, and importantly, this effect was consistent between the two test sites utilizing MRI scanners from different vendors. Regional lobar stiffness measurements similarly demonstrated significant decreases in stiffness with the largest percentile decreases in occipital and the smallest in frontal lobe WM; this may reflect the ventricular dilatation patterns in our patients – a considerable number of our patients had ventricular dilatation of the occipital horns and slit-like frontal horns (ventricular size similarly showed occipital horn volume to be significantly larger than frontal horn volume). This may be a product of the patient population studied; occipital horn dilatation tends to occur in patients who develop hydrocephalus earlier while frontal horn dilatation occurs primarily when hydrocephalus develops later (O'Hayon et al., 1998).

While the group differences in brain stiffness are compelling, and the direction of change – softening of the brain in patients – is very much in line with brain stiffness measurements in other brain pathologies, we also found a number of compelling associations of stiffness measures with demographic and clinical parameters of interest. We will focus on those associations which survived the statistical significance threshold in multivariable regression analyses, indicating an *independent* relationship to brain stiffness outcome measures. Larger ventricular volume was predictive of decreased brain stiffness. Given that lower brain stiffness was found in patients compared to control, and that many studies have shown softer brain tissue to be a surrogate marker of some level of brain pathology (Yin et al., 2018; Streitberger et al., 2012; Murphy et al., 2011; Romano et al., 2014; Lipp et al., 2018; ElSheikh

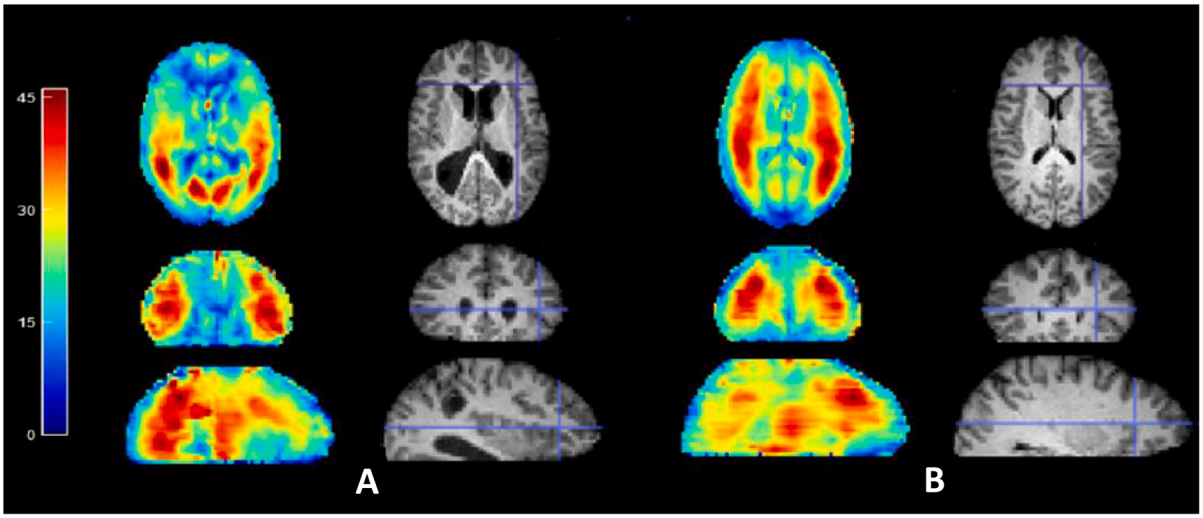

Fig. 3. Representative MRE vibration amplitude images, and corresponding structural images, for a patient (A) and control (B) participant. Wave amplitudes have been summed over all three Cartesian directions to show mean wave amplitude available across the brain for stiffness estimation. Color scale is total brain shear motion in microns.

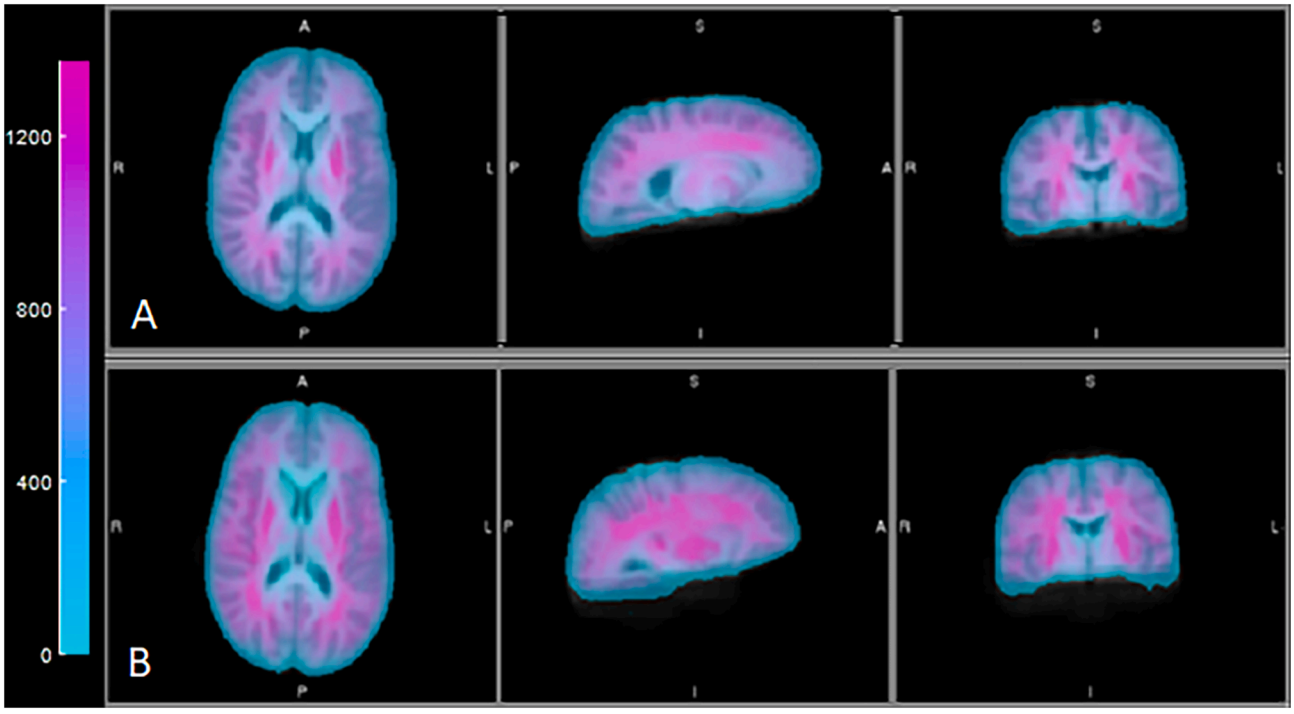

Fig. 4. Average stiffness maps for patients (A) and controls (B). Color scale is mean shear stiffness in Pascal.

Table 2
Global and regional brain stiffness measures from MRE.

G* shear stiffness (Pa)	Hydrocephalus patients (n = 39)	Healthy controls (n = 33)	p-value
Frontal WM	949 (106)	1015 (83)	0.005
Parietal WM	968 (123)	1076 (89)	<0.0001
Occipital WM	871 (140)	986 (75)	<0.0001
Temporal WM	959 (122)	1065 (87)	<0.0001
Whole brain WM	959 (95)	1030 (55)	0.0002
Whole brain	850 (69.77)	930 (43.08)	<0.0001

Values are mean (SD).

et al., 2017), this result suggests a long-term deleterious effect of ventricular dilatation on the cellular structure and biomechanical integrity of overall brain tissue. The relationship with ventricular size was in fact strongest in the occipital lobe, and not significant in the frontal lobe; the majority of ventricular dilatation in our patients was observed in the occipital horns, with many of the patients demonstrating normal to slit-like frontal horns. However, as with any cross-sectional, observational study, we are not able to determine if ventricular dilatation leads to changes in brain stiffness, if other pathological processes lead to brain stiffness changes which in turn may facilitate ventricular dilation or if there is no causal relationship. Furthermore, we are not able to

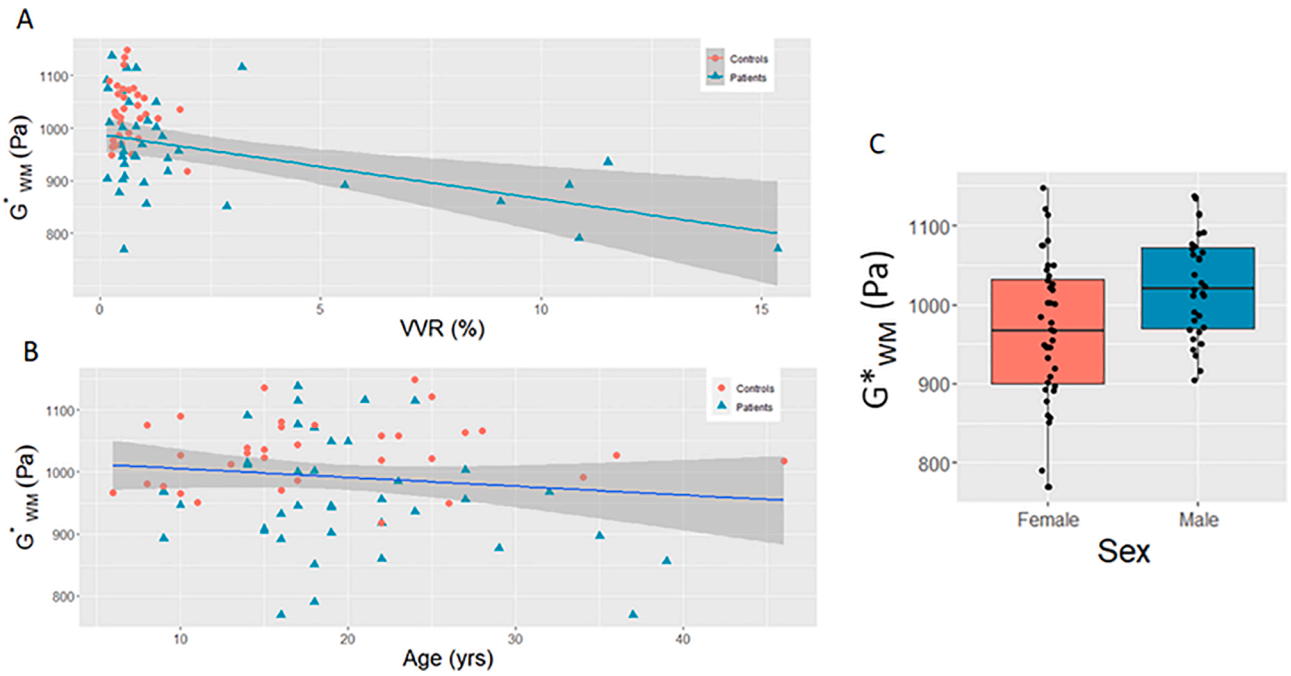

Fig. 5. Relationship between whole white matter shear stiffness and normalized ventricular volume (A), age (B) and Sex (C). Relationship between whole with VVR demonstrates the decreasing brain stiffness in patients with enlarged ventricles, as well as with advanced age. Although the univariate relationships are shown here, these relationships remained as independent predictors of brain stiffness in multivariable regression models.

Table 3
Multivariable linear regression models to compare patients vs. controls. Significant values are in bold.

G*	Frontal WM	Parietal WM	Occipital WM	Temporal WM	WM	WB
Intercept	1090.1 (31.3)	1201.8 (32.3)	1036.4 (33.9)	1175.5 (32.7)	1070.6 (23.5)	1003.3 (22.1)
	<0.0001	<0.0001	<0.0001	<0.0001	<0.0001	<0.0001
Patients vs. controls	**−55.1 (23.3)**	**−79.3 (24.0)**	**−75.5 (25.3)**	**−76.2 (24.3)**	**−42.5 (17.5)**	**−58.2 (16.5)**
	0.0209	**0.0015**	**0.0039**	**0.0025**	**0.018**	**0.0007**
Age	**−3.3 (1.4)**	**−5.7 (1.5)**	−1.7 (1.6)	**−4.8 (1.5)**	−0.9 (1.1)	**−2.9 (1.0)**
	0.0255	**0.0002**	0.2795	**0.0019**	0.4178	**0.0051**
Female vs. male	−29.1 (23.1)	−27.1 (23.8)	−10.7 (25.0)	−31.0 (24.1)	**−36.0 (17.4)**	−30.1 (16.3)
	0.2119	0.259	0.6717	0.2031	**0.0419**	0.07
VVR	−0.4 (4.0)	**−9.2 (4.2)**	**−20.7 (4.4)**	**−9.5 (4.2)**	**−11.9 (3.0)**	**−6.8 (2.8)**
	0.9132	**0.0309**	**<0.0001**	**0.0269**	**0.0002**	**0.0202**

Values listed in the table are beta coefficient (standard error), p value.

Table 4
Multivariable linear regression model including clinical variables, for patients alone. Significant values are in bold.

	Frontal WM	Parietal WM	Occipital WM	Temporal WM	WM	WB
Intercept	1137.1 (49.3)	1266.5 (52.7)	905.7 (63.8)	1131.9 (63.5)	1113.1 (38.9)	1008.7 (38.6)
	<0.0001	<0.0001	<0.0001	<0.0001	<0.0001	<0.0001
Age	−4.2 (2.4)	**−9.5 (2.2)**	−3.7 (2.9)	**−7.6 (2.5)**	−2.8 (1.8)	**−3.7 (1.8)**
	0.0882	**0.0002**	0.2094	**0.004**	0.12	**0.046**
Female vs. male	**−75.6 (34.2)**	−49.2 (31.6)	−42.4 (41.2)	−58.6 (34.9)	**−76.6 (25.5)**	**−73.2 (25.3)**
	0.0342	0.1294	0.3115	0.1031	**0.01**	**0.01**
VVR	1.5 (4.5)	−8.4 (4.2)	**−18.9 (5.4)**	−8.0 (4.6)	**−11.5 (3.4)**	−5.3 (3.3)
	0.7336	0.0506	**0.0014**	0.0904	**0.002**	0.12
Age at shunt [a]	−56.6 (32.8)	−27.1 (30.4)	−44.8 (39.5)	−34.2 (33.5)	−7.3 (24.5)	−21.3 (24.3)
	0.0945	0.3793	0.2658	0.3156	0.77	0.39
Shunt revisions [b]	1.6 (32.5)	−47.2 (30.1)	−26.7 (39.2)	−39.6 (33.2)	−22.9 (24.3)	−19.6 (24.1)
	0.9609	0.1267	0.4999	0.2414	0.35	0.42

Values listed in the table are beta coefficient (standard error), p value.
[a] Age of first shunt was dichotomized at the median age for the patient group (120 days).
[b] Number of revisions was dichotomized at the median number (2 revisions).

differentiate the numerous potential sources for this brain softening – possible candidates may be the initial insult to the brain at the time of the development of ventricular enlargement, the chronic effects of abnormal ventricular size or shunt functionality (Del Bigio et al., 2003), or the pathophysiological changes known to manifest in hydrocephalus patients (Zhang et al., 2017; Del Bigio, 2010, 2004, 2001; Williams et al., 2007). Numerous clinical studies have attempted to use ventricular size as a viable radiological marker to predict hydrocephalus severity, but

Table 5
Association of HOQ, HDI and depression with stiffness measures, using multivariable linear regression model to assess association between HOQ and HDI with each G* measure. Significant values in bold.

G* (Pa)	HOQ	HDI	Depression
Frontal WM	0.0006 (0.0003)	0.0128 (0.0584)	**0.979 (0.959, 1.000)**
	0.07	0.83	**0.048**
Parietal WM	**0.0008 (0.0003)**	0.0999 (0.0572)	**0.982 (0.964, 1.000)**
	0.01	0.09	**0.044**
Occipital WM	0.0003 (0.0002)	0.0745 (0.0422)	0.993 (0.983, 1.002)
	0.32	0.09	0.13
Temporal WM	0.0005 (0.0003)	0.0066 (0.0555)	0.992 (0.981, 1.004)
	0.12	0.91	0.19
WM	**0.0008 (0.0004)**	−0.0640 (0.0723),	**0.972 (0.946, 0.999)**
	0.0497	0.38	**0.040**
WB	**0.0009 (0.0004)**	−0.1004 (0.0714),	**0.972 (0.946, 0.998)**
	0.02	0.17	**0.037**

Values listed in the table (for HOQ and HDI): beta coefficient (Standard error), p value. Values for depression scores: Odds ratios (95% CI), p-value.
All tests were adjusted for age, sex, VVR, age at first shunt and number of revisions. For the depression scores a multivariable logistic regression model was used.

the evidence to date as well as anecdotal observations from several groups indicates that ventricular size is in general a poor predictor of outcome (Buxton et al., 1998; Nikas et al., 2014; Patra et al., 2016; Kim et al., 2000). In contrast, Morales and colleagues have demonstrated that ventriculomegaly is correlated with changes in CSF biomarkers in patients with post-hemorrhagic hydrocephalus of prematurity (Habiyaremye et al., 2017; Limbrick et al., 2017; Morales et al., 2017). There was in fact no relationship between ventricular size and functional outcome in our patients. However, because the majority of our patients did not demonstrate marked ventricular dilatation, further study will be needed to confirm these findings.

Age was similarly predictive of decreased brain stiffness of the frontal, parietal and temporal WM. Specifically, brain stiffness was found to decrease at a rate of approximately 50 Pa/decade. Prior literature on the age dependence of brain stiffness has focused mostly on older adults (Takamura et al., 2019; Arani et al., 2015; Sack et al., 2011; Hiscox et al., 2018), only showing statistically significant declines past 40 years old, with stiffness declines in the range of ~ 50–100 Pa/decade. Similarly, Yeung et al. (2019) found no difference between groups of young children, adolescents and adults (mean age not reported, but the maximum age was 50). We, therefore, found it interesting that age was an independent predictor of stiffness given our mean age of 22 years old. However, these other studies included only healthy individuals, and in our patient cohort the effect sizes of the age-stiffness relationship did increase compared to the entire group as a whole (Table 3 vs. Table 4). WM myelination, which occurs well into adolescence, may present a potential confound to any age-related stiffness changes, but would predict increasing, not decreasing, stiffness with age. Thus, our findings may lend support to the common perception that the brain and cognitive function decline in long-standing shunt-dependent hydrocephalus, which could indicate accelerated, cognitive aging.

Sex was also a significant factor in our cohort, with females exhibiting softer brain tissue compared to males. A number of prior studies have explored sex differences in brain stiffness, but found the opposite or no effect (Sack et al., 2009, 2011; Arani et al., 2015; Hiscox et al., 2018). However, again it is important to note that these other studies were all conducted with healthy subjects. Looking at the different findings from our two models, it is clear that the sex effect sizes were significantly increased when considering patients only, so this sex difference may be specific to our patient population. Within the general context of brain injury, it is generally accepted that women are more susceptible to injury and worse outcome (Cogan et al., 2020; Merritt et al., 2019; Yue et al., 2019; Manley et al., 2017; Cheng et al., 2019; Yumul et al., 2020), although a number of recent studies have begun to question this conclusion (Mollayeva et al., 2018; Choleris et al., 2018). Of course, these results have to be viewed with caution given the relatively small size of our study.

With respect to our two clinical parameters of interest, the age at first shunt and the number of shunt revisions, the conclusions were less compelling. These are both clinical endpoints which have been considered critical in the management of pediatric hydrocephalus. Age at first shunt, and whether or not to delay initial shunting, has been an ongoing debate within the neurosurgical community for decades. The argument can be made in either direction. For example, a recent, multi-center trial concluded that age at first shunt (below vs. above 6 months) was an important factor in determining shunt survival (Riva-Cambrin et al., 2016). On the other hand, studies have shown worse outcome in children shunted later (Del Bigio et al., 1997; McAllister and Chovan, 1998). Similarly, a number of studies have attempted to explore the long-term effects of multiple shunt revisions on clinical outcome, although many studies have not shown significant relationships (Gmeiner et al., 2019; Lindquist et al., 2011; Casey et al., 1997). Our initial univariate analyses did identify an association between age at first shunt, however this relationship did not remain statistically significant in our final multivariable clinical model. It is nonetheless interesting to note that all of the non-significant relationships for both age at shunt and shunt revisions were *negative*, indicating softer brain tissue in patients that were shunted earlier and those with more shunt revisions. Thus, it would certainly be valuable to follow these parameters in larger clinical studies of brain stiffness measures.

Our final model examined the question of whether or not any of the variables studied could be used to predict functional outcome, as measured with health-related quality of life, headache index and depression. These models included total ventricular size, an imaging outcome which is most frequently used by neurosurgeons to manage hydrocephalus patients. Our primary imaging outcome, whole brain WM stiffness, was significant in these models, with increased brain stiffness (*i.e.,* tending to toward normal/control values) being predictive of better health related quality of life and the absence of depression. Prior works have identified predictive relationships between imaging measures, such as diffusion tensor imaging, and outcome, with reliance on longitudinal changes in imaging markers (Mangano et al., 2016). In agreement with our findings, Kulkarni et al. found no association between functional outcome and ventricular size (as well WM integrity measured by DTI) (Kulkarni et al., 2015). Our study used the unique measure of brain stiffness as a predictor of outcome, which has not been explored before in this population; an added strength of our cross-sectional findings in comparison to these studies may be in the multivariable modeling approach to ensure that independent relationships to outcome were properly identified.

Putting these results into the context of traditional views of hydrocephalus, our findings of reduced brain stiffness would appear to contradict both the existing literature as well as the common neurosurgical impression of the hydrocephalic brain being a “tight”, non-compliant system. The neurosurgical literature generally reports intracranial compliance, the inverse of stiffness or elastance. Prior research has exclusively found *reduced* intracranial compliance in patients (Jacobsson et al., 2018; Qvarlander et al., 2014; De Bonis et al., 2013; Greitz, 2007; Bateman, 2002), while our report of decreased stiffness in hydrocephalic patients would imply *increased* not decreased compliance. These disparate findings, however, can be explained from both a methodological and a theoretical standpoint. The intracranial compliance measures noted are almost exclusively assessed via the infusion test, relying on the tight relationship between pressure and volume in the cranium – the pressure–volume curve introduced over forty years ago by Marmarou (Marmarou et al., 1975). By infusing a fixed volume of fluid into the closed craniospinal system and observing the ensuing pressure increase, the intracranial compliance $\Delta V/\Delta P$ is derived. Thus, these measurements only assess the global biomechanical state of the intracranial system as a whole. As such, intracranial

pressure, for example, plays an important role in dictating compliance. On the other hand, MR Elastography as an imaging method assesses the local biomechanical properties of brain tissue. While pressure may play a role in these properties (Arani et al., 2018), MRE measures are primarily dictated by the *local* biomechanical properties of the brain tissue. Recent studies have attempted to devise noninvasive means of measuring ICP (Alperin et al., 2000; Evensen and Eide, 2020; Khan et al., 2017), with the hope of improving patient management without invasive intracranial probes. Our results, however, imply that there may be more to the pathophysiology of hydrocephalus, and by extension perhaps of shunting, than just the global measurement which ICP provides. The more localized changes in brain biomechanics provided by MRE may further our understanding of the changes in the brain which drive outcomes such as shunt failure or chronic, unremitting headache.

Furthermore, while both the infusion test and MRE assess brain stiffness, the two methods assess two very different types of stiffness. The infusion test is a compression-based technique – infusion of volume into the craniospinal compartment compresses everything in the compartment (also see (Shulyakov et al., 2012). Therefore, these tests assess *compressive* brain stiffness. MRE however does not have access to this compressive component; being made up of mostly water, the tissue is at least locally not compressible. MRE instead induces microscopic shear waves in the brain tissue, assessing the softness or stiffness of the tissue to shearing forces, and MRE stiffness measures are thus indicative of *shear* stiffness. Finally, as noted above, there is support from the literature for the notion of brain tissue softening in the presence of brain pathology, such as in Alzheimer's disease (Murphy et al., 2011; ElSheikh et al., 2017; Gerischer et al., 2018) and multiple sclerosis (Wuerfel et al., 2010; Streitberger et al., 2012; Fehlner et al., 2016). More recent MRE investigations in animal models point to the role of astrocytosis (Fehlner et al., 2016; Riek et al., 2012) and changes in neuronal density (Klein et al., 2014) in stiffness reductions. In this light, reduction in brain stiffness in hydrocephalus, or other brain pathologies, can be thought of as a breakdown at the microscopic level of the mechanical integrity of the tissue matrix (Posnansky et al., 2012).

Our results are also in concert with prior investigations using MRE in hydrocephalus, although it is important to note that these studies have been on older adults with so-called normal pressure hydrocephalus (NPH). Freimann et al. (2012) and Streitberger et al. similarly found significant brain wide reduction of MRE-derived stiffness, as well as changes in brain stiffness parameters toward normal following shunt insertion (Streitberger et al., 2010). A recent case report demonstrated that decreased stiffness in a 19-year old patient was reversed two years later by ventriculoperitoneal shunting (Olivero et al., 2020). On the other hand, our results are in contrast with one set of publications, also in NPH patients, which found increased brain stiffness in parietal and occipital cortices but decreased stiffness in periventricular white matter compared to age-matched controls (ElSheikh et al., 2017; Fattahi et al., 2016; Murphy et al., 2020; Perry et al., 2017). These diverging reports highlight the complex nature of hydrocephalus; *e.g.* cytopathology such as periventricular edema and dysmyelination which may drive decreased stiffness (Del Bigio et al., 2003; Del Bigio, 2010), while elevated pressure, which can be intermittent but chronic in NPH, may drive increased stiffness (Pong et al., 2017; Tzschatzsch et al., 2018).

With respect to the pathophysiology of hydrocephalus, the underlying causes are likely multi-factorial (Bergsneider et al., 2006; Del Bigio, 2010; Del Bigio and McAllister, 1999; Bateman, 2007; Dombrowski et al., 2008; Owler et al., 2010; Filippidis et al., 2012; Qvarlander et al., 2013), and the sources of reduced shear stiffness may thus be complicated and difficult to isolate. In addition to local stretching of the periventricular axons (Del Bigio, 2010), there is a reduction in patent capillary blood vessel density (Luciano et al., 2001; Dombrowski et al., 2008), and ensuing reduction in cerebral blood flow, especially in WM (Alperin et al., 2001; Owler et al., 2004; Owler and Pickard, 2001). Recent studies have shown an association between stiffness of deep grey matter structures and the relative cerebral blood flow in each of these structures (Hetzer et al., 2018). Reactive astrocytosis and microglia have been demonstrated in both animal models of hydrocephalus and human pathology (McAllister and Chovan, 1998; Yuan et al., 2010). Hydrocephalus and the associated raised intracranial pressure, especially when it occurs during infancy with rapid myelination and cell proliferation, can affect myelination and brain development (Hanlo et al., 1997; Di Curzio et al., 2013; Khan et al., 2006). While much of this pathology is ameliorated with shunting (Del Bigio, 2001; McAllister et al., 1991; Miller and McAllister, 2007; Del Bigio and Bruni, 1988), even after shunting pathological changes remain (Del Bigio et al., 2003, 1994; Del Bigio, 2001). Further study, and in particular utilizing MRE and animal models of hydrocephalus, will be needed to disentangle these numerous potential contributions to reduced shear stiffness we have demonstrated in patients compared to healthy controls.

The overall conclusions of the study support the notion of impaired WM shear stiffness in early-onset, chronic hydrocephalus patients, as well as a number of compelling associations of this impairment with ventricular size, and demographic and clinical measures. There are a number of limitations to the study, however. The study was cross-sectional and observational, with measurements taken at a single time point later in life in patients who have been living with a functioning shunt for many years. However, this study does form a strong basis for the importance of brain stiffness measurements in the context of hydrocephalus and shunting; follow-up, longitudinal studies will be more powerful in determining the changes in brain stiffness over time in this population, as well as the relationship of temporal changes to shunt-related events, such as shunt failure and emergency room visits. Such studies will be critical to some of the most pressing questions in neurosurgical management of hydrocephalus, such as how brain stiffness is driven by, or is a driving force behind, ventricular expansion at the time of shunt failure, and the optimal pressure setting management following shunt surgery or revision. The number of our patients was relatively small and heterogeneous in etiology, and in particular for the number of patients with moderate to severe ventricular enlargement. Similarly, our analyses were not corrected for multiple comparisons, and possibly prone to false positive rates. However, our use of multivariable regression models allowed assessment of independent associations in which many of the relationships remained highly significant, and certainly point to a number of compelling parameters which should be explored more closely in larger, follow-up studies. Finally, data were collected at two separate sites, and there were significant difference between the sites in terms of age and gender distributions. However, given the difficulty often posed in replicating results across study sites, and in particular for methods which are highly dependent on the details of the MRI-based acquisitions, we were extremely encouraged by the fact that our overall conclusions of reduced WM stiffness could be replicated between the site. Importantly, our secondary analyses confirmed that adjustment for site did not affect our conclusions.

5. Conclusions

MR Elastography is a promising novel noninvasive tool for evaluating changes in the biomechanical properties of brain tissue in hydrocephalus. Brain tissue stiffness is reduced in patients compared to healthy controls, decreases with age and ventricular size, and predicts impairment in terms of overall function measures of quality of life and depression. These changes may be indicative of impaired biomechanical integrity of the brain, either from pathological processes associated with hydrocephalus, or the effects of long-term shunting. Further study will help elucidate the mechanisms behind these relationships, and the changes over time in brain stiffness, or at the time of a clinically-significant event such as shunt failure.

CRediT authorship contribution statement

M.E. Wagshul: Conceptualization, Methodology, Funding

acquisition, Supervision, Formal analysis, Writing - original draft. **J.P. McAllister:** Conceptualization, Funding acquisition, Methodology, Writing - review & editing. **D.D. Limbrick Jr.:** Conceptualization, Supervision, Writing - review & editing. **S. Yang:** Project administration, Data curation, Formal analysis. **W. Mowrey:** Methodology, Writing - review & editing. **J.T. Goodrich:** . **A. Meiri:** Project administration, Data curation. **D.M. Morales:** Project administration, Data curation. **A. Kobets:** Writing - review & editing. **R. Abbott:** Conceptualization, Supervision, Writing - review & editing.

Declaration of Competing Interest

The authors declare that they have no known competing financial interests or personal relationships that could have appeared to influence the work reported in this paper.

Acknowledgements

We would like to acknowledge the assistance of the following individuals: Curtis Johnson (University of Delaware) for help with the MRE pulse sequence at Washington University, Deanna Mercer for help with patient recruitment at Washington University, Maria Robles for help with patient recruitment at Einstein and data organization, and Yisrael Feman for editing and reviewing of the manuscript and assistance with data analysis. We are most grateful to the Rudi Schulte Research Foundation (Santa Barbara, CA) for their financial support of this project. Finally, we want to recognize the help and tireless work of one of our co-authors, Dr. James Goodrich, who unfortunately passed away in the midst of the COVID pandemic and was not able to participate in the drafting of this manuscript. He showed us all what it means to be an exemplary clinician, researcher and human being, a true global citizen. We, and the entire neurosurgical community, will miss him dearly.

References

Alperin, N.J., et al., 2000. MR-Intracranial pressure (ICP): a method to measure intracranial elastance and pressure noninvasively by means of MR imaging: baboon and human study. Radiology 217 (3), 877–885.
Alperin, N., et al., 2001. Analysis of magnetic resonance imaging-based blood and cerebrospinal fluid flow measurements in patients with Chiari I malformation: a system approach. Neurosurg. Focus 11 (1), E6.
Arani, A., et al., 2015. Measuring the effects of aging and sex on regional brain stiffness with MR elastography in healthy older adults. Neuroimage 111, 59–64.
Arani, A., et al., 2018. Acute pressure changes in the brain are correlated with MR elastography stiffness measurements: initial feasibility in an in vivo large animal model. Magn. Reson. Med. 79 (2), 1043–1051.
Arunachalam, S.P., et al., 2017. Quantitative 3D magnetic resonance elastography: comparison with dynamic mechanical analysis. Magn. Reson. Med. 77 (3), 1184–1192.
Assaf, Y., et al., 2006. Diffusion tensor imaging in hydrocephalus: initial experience. AJNR Am. J. Neuroradiol. 27 (8), 1717–1724.
Avants, B.B., et al., 2011. A reproducible evaluation of ANTs similarity metric performance in brain image registration. Neuroimage 54 (3), 2033–2044.
Bang, Y.R., Park, J.H., Kim, S.H., 2015. Cut-off scores of the children's depression inventory for screening and rating severity in Korean adolescents. Psychiatry Investig. 12 (1), 23–28.
Bateman, G.A., 2002. Pulse-wave encephalopathy: a comparative study of the hydrodynamics of leukoaraiosis and normal-pressure hydrocephalus. Neuroradiology 44 (9), 740–748.
Bateman, G.A., 2007. The pathophysiology of idiopathic normal pressure hydrocephalus: cerebral ischemia or altered venous hemodynamics? AJNR Am. J. Neuroradiol.
Ben-Sira, L., et al., 2015. Clinical benefits of diffusion tensor imaging in hydrocephalus. J. Neurosurg. Pediatr. 16 (2), 195–202.
Bergsneider, M., et al., 2006. What we don't (but should) know about hydrocephalus. J. Neurosurg. 104 (3 Suppl), 157–159.
Boyer, K.M., Yeates, K.O., Enrile, B.G., 2006. Working memory and information processing speed in children with myelomeningocele and shunted hydrocephalus: analysis of the children's paced auditory serial addition test. J. Int. Neuropsychol. Soc. 12 (3), 305–313.
Bradley Jr, W.G., et al., 1996. Normal-pressure hydrocephalus: evaluation with cerebrospinal fluid flow measurements at MR imaging. Radiology 198 (2), 523–529.
Braun, J., et al., 2014. High-resolution mechanical imaging of the human brain by three-dimensional multifrequency magnetic resonance elastography at 7T. Neuroimage 90, 308–314.
Buxton, N., et al., 1998. Neuroendoscopy in the premature population. Childs Nerv. Syst. 14 (11), 649–652.
Buxton, N., et al., 1998. Neuroendoscopic third ventriculostomy in patients less than 1 year old. Pediatr. Neurosurg. 29 (2), 73–76.
Casey, A.T., et al., 1997. The long-term outlook for hydrocephalus in childhood. A ten-year cohort study of 155 patients. Pediatr. Neurosurg. 27 (2), 63–70.
Cheng, J., et al., 2019. Sex-based differences in the incidence of sports-related concussion: systematic review and meta-analysis. Sports Health 11 (6), 486–491.
Choleris, E., et al., 2018. Sex differences in the brain: implications for behavioral and biomedical research. Neurosci. Biobehav. Rev. 85, 126–145.
Clayton, E.H., Okamoto, R.J., Bayly, P.V., 2013. Mechanical properties of viscoelastic media by local frequency estimation of divergence-free wave fields. J. Biomech. Eng. 135 (2), 021025.
Cogan, A.M., McCaughey, V.K., Scholten, J., 2020. Gender differences in outcomes after traumatic brain injury among service members and veterans. PM R 12 (3), 301–314.
De Bonis, P., et al., 2013. CSF dynamics analysis in patients with post-traumatic ventriculomegaly. Clin. Neurol. Neurosurg. 115 (1), 49–53.
Del Bigio, M.R., et al., 1994. Acute and chronic cerebral white matter damage in neonatal hydrocephalus. Can. J. Neurol. Sci. 21 (4), 299–305.
Del Bigio, M.R., 2004. Cellular damage and prevention in childhood hydrocephalus. Brain Pathol. 14 (3), 317–324.
Del Bigio, M.R., 2010. Neuropathology and structural changes in hydrocephalus. Dev. Disabil. Res. Rev. 16 (1), 16–22.
Del Bigio, M.R., McAllister, J.P.I. (Eds.), 1999. Pathophysiology of Hydrocephalus. Pediatric Neurosurgery, ed. C. M., et al. 1999, Churchill Livingstone. Philadelphia, pp. 217–236.
Del Bigio, M.R., Bruni, J.E., 1988. Periventricular pathology in hydrocephalic rabbits before and after shunting. Acta Neuropathol. 77 (2), 186–195.
Del Bigio, M.R., Crook, C.R., Buist, R., 1997. Magnetic resonance imaging and behavioral analysis of immature rats with kaolin-induced hydrocephalus: pre- and postshunting observations. Exp. Neurol. 148 (1), 256–264.
Del Bigio, M.R., Wilson, M.J., Enno, T., 2003. Chronic hydrocephalus in rats and humans: white matter loss and behavior changes. Ann. Neurol. 53 (3), 337–346.
Del Bigio, M.R., 2001. Pathophysiologic consequences of hydrocephalus. Neurosurg. Clin. N. Am. 12(4), 639–649, vii.
Di Curzio, D.L., Buist, R.J., Del Bigio, M.R., 2013. Reduced subventricular zone proliferation and white matter damage in juvenile ferrets with kaolin-induced hydrocephalus. Exp. Neurol. 248, 112–128.
Dombrowski, S.M., et al., 2008. Chronic hydrocephalus-induced hypoxia: increased expression of VEGFR-2+ and blood vessel density in hippocampus. Neuroscience 152 (2), 346–359.
Ehman, E.C., et al., 2008. Vibration safety limits for magnetic resonance elastography. Phys. Med. Biol. 53 (4), 925–935.
ElSheikh, M., et al., 2017. MR Elastography demonstrates unique regional brain stiffness patterns in dementias. AJR Am. J. Roentgenol. 209 (2), 403–408.
Evensen, K.B., Eide, P.K., 2020. Measuring intracranial pressure by invasive, less invasive or non-invasive means: limitations and avenues for improvement. Fluids Barriers CNS 17 (1), 34.
Fattahi, N., et al., 2016. MR Elastography demonstrates increased brain stiffness in normal pressure hydrocephalus. AJNR Am. J. Neuroradiol. 37 (3), 462–467.
Fehlner, A., et al., 2016. Higher-resolution MR elastography reveals early mechanical signatures of neuroinflammation in patients with clinically isolated syndrome. J. Magn. Reson. Imaging 44 (1), 51–58.
Fehlner, A., et al., 2017. Increasing the spatial resolution and sensitivity of magnetic resonance elastography by correcting for subject motion and susceptibility-induced image distortions. J. Magn. Reson. Imaging 46 (1), 134–141.
Filippidis, A.S., Kalani, M.Y., Rekate, H.L., 2012. Hydrocephalus and aquaporins: the role of aquaporin-4. Acta Neurochir. Suppl. 113, 55–58.
Fletcher, J.M., Barnes, M., Dennis, M., 2002. Language development in children with spina bifida. Semin. Pediatr. Neurol. 9 (3), 201–208.
Fovargue, D., Nordsletten, D., Sinkus, R., 2018. Stiffness reconstruction methods for MR elastography. NMR Biomed. 31 (10), e3935.
Freimann, F.B., et al., 2012. Alteration of brain viscoelasticity after shunt treatment in normal pressure hydrocephalus. Neuroradiology 54 (3), 189–196.
Gerischer, L.M., et al., 2018. Combining viscoelasticity, diffusivity and volume of the hippocampus for the diagnosis of Alzheimer's disease based on magnetic resonance imaging. Neuroimage Clin. 18, 485–493.
Gigi, M., et al., 2019. Health-related quality of life after post-haemorrhagic hydrocephalus in children born preterm. Dev. Med. Child Neurol. 61 (3), 343–349.
Gmeiner, M., et al., 2019. Adult outcome in shunted pediatric hydrocephalus: long-term functional, social, and neurocognitive results. World Neurosurg. 132, e314–e323.
Greitz, D., 2007. Paradigm shift in hydrocephalus research in legacy of Dandy's pioneering work: rationale for third ventriculostomy in communicating hydrocephalus. Childs Nerv. Syst. 23 (5), 487–489.
Guo, J., et al., 2013. Towards an elastographic atlas of brain anatomy. PLoS ONE 8 (8), e71807.
Habiyaremye, G., et al., 2017. Chemokine and cytokine levels in the lumbar cerebrospinal fluid of preterm infants with post-hemorrhagic hydrocephalus. Fluids Barriers CNS 14 (1), 35.
Hanlo, P.W., et al., 1997. The effect of intracranial pressure on myelination and the relationship with neurodevelopment in infantile hydrocephalus. Dev. Med. Child Neurol. 39 (5), 286–291.
Harris, P.A., et al., 2009. Research electronic data capture (REDCap)—a metadata-driven methodology and workflow process for providing translational research informatics support. J. Biomed. Inform. 42 (2), 377–381.

Hetzer, S., et al., 2018. Perfusion alters stiffness of deep gray matter. J. Cereb. Blood Flow Metab. 38 (1), 116–125.
Hirsch, S., et al., 2014. MR elastography of the liver and the spleen using a piezoelectric driver, single-shot wave-field acquisition, and multifrequency dual parameter reconstruction. Magn. Reson. Med. 71 (1), 267–277.
Hirsch, S., Braun, J., Sack, I., 2017. Magnetic resonance Elastography: physical background and medical applications. Weinheim, Germany, Wiley-VCH Verlag, p. 456.
Hiscox, L.V., et al., 2018. High-resolution magnetic resonance elastography reveals differences in subcortical gray matter viscoelasticity between young and healthy older adults. Neurobiol. Aging 65, 158–167.
Hofmann, E., et al., 1995. The corpus callosum in communicating and noncommunicating hydrocephalus. Neuroradiology 37 (3), 212–218.
Houtrow, A.J., Burrows, P.K., Thom, E.A., 2018. Comparing neurodevelopmental outcomes at 30 months by presence of hydrocephalus and shunt status among children enrolled in the MOMS trial. J. Pediatr. Rehabil. Med. 11 (4), 227–235.
Jacobson, G.P., et al., 1995. Headache Disability Inventory (HDI): short-term test-retest reliability and spouse perceptions. Headache: J. Head Face Pain 35 (9), 534–539.
Jacobsson, J., et al., 2018. Comparison of the CSF dynamics between patients with idiopathic normal pressure hydrocephalus and healthy volunteers. J. Neurosurg. 1–6.
Jang, S.H., et al., 2013. The effects of hydrocephalus on the periventricular white matter in intracerebral hemorrhage: a diffuser tensor imaging study. Int. J. Neurosci. 123 (6), 420–424.
Johnson, C.L., et al., 2013. Local mechanical properties of white matter structures in the human brain. Neuroimage 79, 145–152.
Kahlon, B., et al., 2007. Is aqueductal stroke volume, measured with cine phase-contrast magnetic resonance imaging scans useful in predicting outcome of shunt surgery in suspected normal pressure hydrocephalus? Neurosurgery, 60(1), 124–129; discussion 129-30.
Kang, K., et al., 2018. Lateral ventricle enlargement and cortical thinning in idiopathic normal-pressure hydrocephalus patients. Sci. Rep. 8 (1), 13306.
Kao, C.L., et al., 2001. The outcome of shunted hydrocephalic children. Zhonghua Yi Xue Za Zhi (Taipei) 64 (1), 47–53.
Khan, M.N., et al., 2017. Noninvasive monitoring intracranial pressure - a review of available modalities. Surg. Neurol. Int. 8, 51.
Khan, O.H., Enno, T.L., Del Bigio, M.R., 2006. Brain damage in neonatal rats following kaolin induction of hydrocephalus. Exp. Neurol. 200 (2), 311–320.
Kim, S.K., Wang, K.C., Cho, B.K., 2000. Surgical outcome of pediatric hydrocephalus treated by endoscopic III ventriculostomy: prognostic factors and interpretation of postoperative neuroimaging. Childs Nerv. Syst. 16 (3), 161–168 discussion 169.
Klein, C., et al., 2014. Enhanced adult neurogenesis increases brain stiffness: in vivo magnetic resonance elastography in a mouse model of dopamine depletion. PLoS ONE 9 (3), e92582.
Kovacs, M., 1985. The children's depression, inventory (CDI). Psychopharmacol. Bull. 21 (4), 995–998.
Kruse, S.A., et al., 2008. Magnetic resonance elastography of the brain. Neuroimage 39 (1), 231–237.
Kulkarni, A.V., et al., 2008. Comparing children's and parents' perspectives of health outcome in paediatric hydrocephalus. Dev. Med. Child Neurol. 50 (8), 587–592.
Kulkarni, A.V., et al., 2015. Relationship between ventricular size, white matter injury, and neurocognition in children with stable, treated hydrocephalus. J. Neurosurg. Pediatr. 16 (3), 267–274.
Kulkarni, A.V., Rabin, D., Drake, J.M., 2004. An instrument to measure the health status in children with hydrocephalus: the Hydrocephalus Outcome Questionnaire. J. Neurosurg. 101 (2 Suppl), 134–140.
Lacy, M., et al., 2008. Intellectual functioning in children with early shunted posthemorrhagic hydrocephalus. Pediatr. Neurosurg. 44 (5), 376–381.
Leinonen, V., Vanninen, R., Rauramaa, T., 2017. Cerebrospinal fluid circulation and hydrocephalus. Handb. Clin. Neurol. 145, 39–50.
Limbrick Jr, D.D., et al., 2017. Cerebrospinal fluid biomarkers of pediatric hydrocephalus. Pediatr. Neurosurg. 52 (6), 426–435.
Lindquist, B., et al., 2011. Very long-term follow-up of cognitive function in adults treated in infancy for hydrocephalus. Childs Nerv. Syst. 27 (4), 597–601.
Lipp, A., et al., 2018. Progressive supranuclear palsy and idiopathic Parkinson's disease are associated with local reduction of in vivo brain viscoelasticity. Eur. Radiol. 28 (8), 3347–3354.
Luciano, M.G., et al., 2001. Cerebrovascular adaptation in chronic hydrocephalus. J. Cereb. Blood Flow Metab. 21 (3), 285–294.
Luetmer, P.H., et al., 2002. Measurement of cerebrospinal fluid flow at the cerebral aqueduct by use of phase-contrast magnetic resonance imaging: technique validation and utility in diagnosing idiopathic normal pressure hydrocephalus. Neurosurgery, 50(3), 534–543; discussion 543-4.
Lutkenhoff, E.S., et al., 2014. Optimized brain extraction for pathological brains (optiBET). PLoS ONE 9 (12), e115551.
Manduca, A., et al., 2001. Magnetic resonance elastography: non-invasive mapping of tissue elasticity. Med. Image Anal. 5 (4), 237–254.
Mangano, F.T., et al., 2016. Diffusion tensor imaging study of pediatric patients with congenital hydrocephalus: 1-year postsurgical outcomes. J. Neurosurg. Pediatr. 18 (3), 306–319.
Manley, G., et al., 2017. A systematic review of potential long-term effects of sport-related concussion. Br. J. Sports Med. 51 (12), 969–977.
Marmarou, A., Shulman, K., LaMorgese, J., 1975. Compartmental analysis of compliance and outflow resistance of the cerebrospinal fluid system. J. Neurosurg. 43 (5), 523–534.
McAllister 2nd, J.P., et al., 1991. Progression of experimental infantile hydrocephalus and effects of ventriculoperitoneal shunts: an analysis correlating magnetic resonance imaging with gross morphology. Neurosurgery 29 (3), 329–340.
McAllister 2nd, J.P., Chovan, P., 1998. Neonatal hydrocephalus. Mechanisms and consequences. Neurosurg. Clin. N. Am. 9 (1), 73–93.
McGarry, M.D., et al., 2011. An octahedral shear strain-based measure of SNR for 3D MR elastography. Phys. Med. Biol. 56 (13), N153–N164.
Merritt, V.C., Padgett, C.R., Jak, A.J., 2019. A systematic review of sex differences in concussion outcome: what do we know? Clin. Neuropsychol. 33 (6), 1016–1043.
Miller, J.M., McAllister 2nd, J.P., 2007. Reduction of astrogliosis and microgliosis by cerebrospinal fluid shunting in experimental hydrocephalus. Cerebrospinal Fluid Res. 4, 5.
Mollayeva, T., Mollayeva, S., Colantonio, A., 2018. Traumatic brain injury: sex, gender and intersecting vulnerabilities. Nat. Rev. Neurol. 14 (12), 711–722.
Morales, D.M., et al., 2017. Lumbar cerebrospinal fluid biomarkers of posthemorrhagic hydrocephalus of prematurity: amyloid precursor protein, soluble amyloid precursor protein alpha, and L1 cell adhesion molecule. Neurosurgery 80 (1), 82–90.
Mouton Paradot, G., et al., 2010. Contribution of phase-contrast MRI to the management of patients with normal pressure hydrocephalus: can it predict response to shunting? Neurochirurgie.
Murphy, M.C., et al., 2011. Decreased brain stiffness in Alzheimer's disease determined by magnetic resonance elastography. J. Magn. Reson. Imaging 34 (3), 494–498.
Murphy, M.C., et al., 2013. Measuring the characteristic topography of brain stiffness with magnetic resonance elastography. PLoS ONE 8 (12), e81668.
Murphy, M.C., et al., 2020. Identification of normal pressure hydrocephalus by disease-specific patterns of brain stiffness and damping ratio. Invest. Radiol. 55 (4), 200–208.
Nikas, D.C., et al., 2014. Pediatric hydrocephalus: systematic literature review and evidence-based guidelines. Part 10: Change in ventricle size as a measurement of effective treatment of hydrocephalus. J. Neurosurg. Pediatr. 14 (Suppl 1), 77–81.
O'Hayon, B.B., et al., 1998. Frontal and occipital horn ratio: a linear estimate of ventricular size for multiple imaging modalities in pediatric hydrocephalus. Pediatr. Neurosurg. 29 (5), 245–249.
Oishi, K., et al., 2009. Atlas-based whole brain white matter analysis using large deformation diffeomorphic metric mapping: application to normal elderly and Alzheimer's disease participants. Neuroimage 46 (2), 486–499.
Olivero, W.C., et al., 2020. Brain stiffness following recovery in a patient with an episode of low-pressure hydrocephalus: case report. Childs Nerv. Syst.
Owler, B.K., et al., 2004. Normal pressure hydrocephalus and cerebral blood flow: a PET study of baseline values. J. Cereb. Blood Flow Metab. 24 (1), 17–23.
Owler, B.K., Pickard, J.D., 2001. Normal pressure hydrocephalus and cerebral blood flow: a review. Acta Neurol. Scand. 104 (6), 325–342.
Owler, B.K., Pitham, T., Wang, D., 2010. Aquaporins: relevance to cerebrospinal fluid physiology and therapeutic potential in hydrocephalus. Cerebrospinal Fluid Res. 7, 15.
Patra, D.P., et al., 2016. Role of radiological parameters in predicting overall shunt outcome after ventriculoperitoneal shunt insertion in pediatric patients with obstructive hydrocephalus. Neurosurg. Focus 41 (5), E4.
Perry, A., et al., 2017. Clinical correlation of abnormal findings on magnetic resonance elastography in idiopathic normal pressure hydrocephalus. World Neurosurg. 99, 695–700 e1.
Platenkamp, M., et al., 2007. Outcome in pediatric hydrocephalus: a comparison between previously used outcome measures and the hydrocephalus outcome questionnaire. J. Neurosurg. 107 (1 Suppl), 26–31.
Pong, A.C., et al., 2017. Development of acute hydrocephalus does not change brain tissue mechanical properties in adult rats, but in juvenile rats. PLoS ONE 12 (8), e0182808.
Posnansky, O., et al., 2012. Fractal network dimension and viscoelastic powerlaw behavior: I. A modeling approach based on a coarse-graining procedure combined with shear oscillatory rheometry. Phys. Med. Biol. 57 (12), 4023–4040.
Qvarlander, S., et al., 2013. Pulsatility in CSF dynamics: pathophysiology of idiopathic normal pressure hydrocephalus. J. Neurol. Neurosurg. Psychiatry 84 (7), 735–741.
Qvarlander, S., Malm, J., Eklund, A., 2014. CSF dynamic analysis of a predictive pulsatility-based infusion test for normal pressure hydrocephalus. Med. Biol. Eng. Comput. 52 (1), 75–85.
Rajagopal, A., et al., 2013. White matter microstructural abnormality in children with hydrocephalus detected by probabilistic diffusion tractography. AJNR Am. J. Neuroradiol. 34 (12), 2379–2385.
Riek, K., et al., 2012. Magnetic resonance elastography reveals altered brain viscoelasticity in experimental autoimmune encephalomyelitis. Neuroimage Clin. 1 (1), 81–90.
Riva-Cambrin, J., et al., 2016. Risk factors for shunt malfunction in pediatric hydrocephalus: a multicenter prospective cohort study. J. Neurosurg. Pediatr. 17 (4), 382–390.
Romano, A., et al., 2014. In vivo waveguide elastography: effects of neurodegeneration in patients with amyotrophic lateral sclerosis. Magn. Reson. Med. 72 (6), 1755–1761.
Sack, I., et al., 2009. The impact of aging and gender on brain viscoelasticity. Neuroimage 46 (3), 652–657.
Sack, I., et al., 2011. The influence of physiological aging and atrophy on brain viscoelastic properties in humans. PLoS ONE 6 (9), e23451.
Shulyakov, A.V., Buist, R.J., Del Bigio, M.R., 2012. Intracranial biomechanics of acute experimental hydrocephalus in live rats. Neurosurgery 71 (5), 1032–1040.
Smith, S.M., et al., 2004. Advances in functional and structural MR image analysis and implementation as FSL. Neuroimage 23 (Suppl 1), S208–S219.

Streitberger, K.J., et al., 2010. In vivo viscoelastic properties of the brain in normal pressure hydrocephalus. NMR Biomed.
Streitberger, K.J., et al., 2012. Brain viscoelasticity alteration in chronic-progressive multiple sclerosis. PLoS ONE 7 (1), e29888.
Streitberger, K.J., et al., 2014. High-resolution mechanical imaging of glioblastoma by multifrequency magnetic resonance elastography. PLoS ONE 9 (10), e110588.
Takamura, T., et al., 2019. Influence of age on global and regional brain stiffness in young and middle-aged adults. J. Magn. Reson. Imaging.
Tan, K., et al., 2018. Diffusion tensor imaging and ventricle volume quantification in patients with chronic shunt-treated hydrocephalus: a matched case-control study. J. Neurosurg. 129 (6), 1611–1622.
Thabrew, H., et al., 2017. Systematic review of screening instruments for psychosocial problems in children and adolescents with long-term physical conditions. Glob. Pediatr. Health, 4, 2333794X17690314.
Tzschatzsch, H., et al., 2018. In vivo time-harmonic ultrasound elastography of the human brain detects acute cerebral stiffness changes induced by intracranial pressure variations. Sci. Rep. 8 (1), 17888.
Venkatesh, S.K., Yin, M., Ehman, R.L., 2013. Magnetic resonance elastography of liver: technique, analysis, and clinical applications. J. Magn. Reson. Imaging 37 (3), 544–555.
Wang, Y.P., Gorenstein, C., 2013. Psychometric properties of the Beck Depression Inventory-II: a comprehensive review. Braz. J. Psychiatry 35 (4), 416–431.
Williams, M.A., et al., 2007. Priorities for hydrocephalus research: report from a National Institutes of Health-sponsored workshop. J. Neurosurg. 107 (5 Suppl), 345–357.
Wuerfel, J., et al., 2010. MR-elastography reveals degradation of tissue integrity in multiple sclerosis. Neuroimage 49 (3), 2520–2525.
Yeung, J., et al., 2019. Paediatric brain tissue properties measured with magnetic resonance elastography. Biomech. Model. Mechanobiol.
Yin, Z., et al., 2018. Stiffness and beyond: what MR elastography can tell us about brain structure and function under physiologic and pathologic conditions. Top. Magn. Reson. Imaging 27 (5), 305–318.
Yuan, W., et al., 2009. Anisotropic diffusion properties in infants with hydrocephalus: a diffusion tensor imaging study. AJNR Am. J. Neuroradiol. 30 (9), 1792–1798.
Yuan, W., et al., 2010. Diffusion tensor imaging correlates with cytopathology in a rat model of neonatal hydrocephalus. Cerebrospinal Fluid Res. 7 (1), 19.
Yuan, W., et al., 2013. Diffusion tensor imaging properties and neurobehavioral outcomes in children with hydrocephalus. AJNR Am. J. Neuroradiol. 34 (2), 439–445.
Yuan, W., et al., 2016. Left hemisphere structural connectivity abnormality in pediatric hydrocephalus patients following surgery. Neuroimage Clin. 12, 631–639.
Yue, J.K., et al., 2019. Age and sex-mediated differences in six-month outcomes after mild traumatic brain injury in young adults: a TRACK-TBI study. Neurol. Res. 41 (7), 609–623.
Yumul, J.N., et al., 2020. Concussive symptoms following pediatric mild traumatic brain injury. J. Head Trauma Rehabil.
Zhang, S., et al., 2017. Alterations in cortical thickness and white matter integrity in mild-to-moderate communicating hydrocephalic school-aged children measured by whole-brain cortical thickness mapping and DTI. Neural Plast. 2017, 5167973.
Zhang, Y., Brady, M., Smith, S., 2001. Segmentation of brain MR images through a hidden Markov random field model and the expectation-maximization algorithm. IEEE Trans. Med. Imaging 20 (1), 45–57.